Crystalline assembly of perylene in metal–organic framework thin film: J-aggregate or excimer? Insight into the electronic structure

Mariana Kozlowska[1,6], **Yohanes Pramudya**[1,6], **Marius Jakoby**[2], **Shahriar Heidrich**[1], **Liuyang Pan**[3,4], **Bryce S Richards**[2,5], **Ian A Howard**[2,5], **Christof Wöll**[3], **Ritesh Haldar**[3,*] **and Wolfgang Wenzel**[1,*]

[1] Karlsruhe Institute of Technology, Institute of Nanotechnology, Hermann-von-Helmholtz Platz-1, 76344 Eggenstein-Leopoldshafen, Germany
[2] Karlsruhe Institute of Technology, Institute of Microstructure Technology, Hermann-von-Helmholtz Platz-1, 76344 Eggenstein-Leopoldshafen, Germany
[3] Karlsruhe Institute of Technology, Institute of Functional Interfaces, Hermann-von-Helmholtz Platz-1, 76344 Eggenstein-Leopoldshafen, Germany
[4] Institute of Precision Optical Engineering, School of Physics Science and Engineering, Tongji University, Shanghai, 200092, People's Republic of China
[5] Karlsruhe Institute of Technology (KIT), Light Technology Institute (LTI), Engesserstrasse 13, Karlsruhe, 76131, Germany

E-mail: ritesh.haldar@kit.edu and wolfgang.wenzel@kit.edu

Abstract

The spatial orientation of chromophores defines the photophysical and optoelectronic properties of a material and serves as the main tunable parameter for tailoring functionality. Controlled assembly for achieving a predefined spatial orientation of chromophores is rather challenging. Metal–organic frameworks (MOFs) are an attractive platform for exploring the virtually unlimited chemical space of organic components and their self-assembly for device optimization. Here, we demonstrate the impact of interchromophore interactions on the photophysical properties of a surface-anchored MOF (SURMOF) based on 3,9-perylenedicarboxylicacid linkers. We predict the structural assembly of the perylene molecules in the MOF via robust periodic density functional theory calculations and discuss the impact of unit topology and $\pi-\pi$ interaction patterns on spectroscopic and semiconducting properties of the MOF films. We explain the dual nature of excited states in the perylene MOF, where strong temperature-modulated excimer emission, enhanced by the formation of perylene J-aggregates, and low stable monomer emission are observed. We use band-like and hopping transport mechanisms to predict semiconducting properties of perylene SURMOF-2 films as a function of inter-linker interactions, demonstrating both p-type and n-type conduction mechanisms. Hole carrier mobility up to 7.34 cm^2 Vs^{-1} is predicted for the perylene SURMOF-2. The results show a promising pathway towards controlling excimer photophysics in a MOF while controlling charge carrier mobility on the basis of a predictive model.

1. Introduction

Tailoring of the optical and electronic structures of organic materials is challenging, because the condensed state behavior of large π-surfaces containing organic chromophores/semiconductors is difficult to control. van der Waals interactions are the decisive parameters that control the condensed state geometry of organic molecules, and these remain hard to predict [1]. This poses several barriers to the use of organic materials in optoelectronic applications, including: (a) nonradiative deactivation of the photoexcitation, leading to fluorescence quenching [2]; and (b) electronic states with strongly bound electron–hole pairs, which reduce charge carrier mobility/conductivity. A combination of strong fluorescence emission and high charge carrier mobility could be beneficial for the development of efficient organic light-emitting diodes, organic light emitting transistors, electrically pumped organic lasers, etc. Indeed, charge carrier mobility is often enhanced by densely ordered molecular packing, but this may quench emission owing to aggregation [3–5]. However, both processes can be linked by using molecular engineering to tailor the subtle structural components of molecules, thereby influencing their individual electronic properties and intermolecular electronic communication [6, 7]. Therefore, to overcome these challenges, new design strategies for condensed state behavior are necessary.

The limitations of unpredictable self-assembly can be minimized by a particularly interesting approach involving a metal–organic framework (MOF) [3]. Using an isoreticular synthetic strategy, a directional coordination bond between a suitably functionalized organic linker and a metal/metal-oxo node can be tethered to obtain an ordered framework structure [4, 5]. The periodic assembly can be designed, and a virtually unlimited number of such frameworks can be built for various applications, including gas storage [6] and separation [7–10], catalysis [11, 12], sensing [13a], spintronics [13b] and optoelectronics [14]. In particular, any optically active organic chromophore (or any semiconductor) with suitable functionalization can be integrated into the MOF structure, allowing for controllable periodic assembly. This also provides opportunities for investigating unique optical and electronic properties by quantum mechanical methods [15–17]. Virtual design of optically active linkers and their condensed phase geometry can help to tailor MOF-based devices for applications in diodes, sensors, photoswitches, photovoltaics, etc. Straightforward control over a material's nanostructure and properties becomes possible, whereas this is difficult to achieve with conventional self-assembled amorphous materials.

The number of MOFs with optically active linkers and potential for optoelectronic applications is rather large. However, conventional powder crystalline forms are not suitable for optical and electrical characterization or device implementation. This limitation can be overcome by monolithic thin film fabrication [18], in particular, the layer-by-layer liquid-phase epitaxy [18d] method has attracted much attention. Using this method, MOFs can be deposited as a crystalline oriented monolith on the desired substrate with control over thickness [19]. This monolithic MOF film, known as a surface-anchored MOF (SURMOF), is ideally suited to applications including energy harvesting, nonlinear optics, optical coating, photoresponsive smart materials, and membranes. In the present work, we explore a SURMOF thin film of a well-known perylene chromophore. To construct the MOF structure using perylene, we used dicarboxylate functionalized 3,9-perylenedicarboxylicacid (PDC).

Among the available optically active chromophores, perylene is an attractive candidate. With its substantial and highly delocalized π-electron density, perylene exhibits strong fluorescence in the solution state. However, strong inter-perylene interactions in a randomly arranged or amorphous condensed phase often lead to formation of non-emissive H-aggregates [20]. Loss of radiative energy and short-lived localized charge in the condensed phase of perylene are the primary barriers that must be overcome to achieve high-efficiency performance in optoelectronic device applications.

Perylene can be assembled in a MOF in a periodic and adjustable condensed phase structure with promising optical and electronic features [20–24]. Here, we chose a class of SURMOF structures, known as SURMOF-2 [25], in which perylene chromophores can be assembled in a continuously $\pi-\pi$-stacked fashion [23]. Such an arrangement allows for strong inter-chromophore coupling [26] and delocalization of the photoexcited state over many chromophores, at a length of >100 nm [17, 27]. Therefore, in SURMOF-2, substantial changes in the optical and electronic properties of perylene are expected [28–30]. In the present study, we demonstrate a Zn-PDC SURMOF-2-type structure, which shows red-shifted absorption and emission features compared with those observed in the solvated state of PDC. To elucidate the origins of the optical properties and estimate the potential of the PDC assembly as a semiconductor, we utilize *ab initio* quantum

mechanical calculations. In-depth experimental characterization and density functional theory (DFT) analyses reveal the key features of the perylene assembly in the SURMOF-2 structure for J-type exciton coupling. A suitable structural model for the observed optical and electronic features is also postulated.

2. Experimental and computational setup

2.1. Zn-PDC SURMOF fabrication

Zn-PDC [23] SURMOF-2 (labeled as 'SURMOF' in the text) was fabricated by a layer-by-layer spin coating method, following a previously established method [27]. An ethanolic solution of zinc acetate (1 mM) and a PDC linker (20 μM) were deposited alternately on a precleaned substrate (glass/SiO$_2$) by spin coating. After each metal/linker deposition step, the sample was rinsed with ethanol to remove unreacted precursors and side products. This procedure was repeated to achieve the desired thickness of the thin film. Spin coating was performed at a speed of 2000 rpm. The experimental and simulated x-ray diffraction patterns are shown in figure S1 (https://stacks.iop.org/JPCM/33/034001/mmedia).

2.2. Computational details

To shed light on the microscopic parameters of perylene chromophores in Zn-PDC (figure 1), DFT calculations were performed using both cluster and periodic approaches. A periodic MOF structure was optimized with the dispersion-corrected SCAN + rVV10 meta-GGA [31, 32] functional using the Vienna *ab initio* simulation package [33] (VASP 5.4.4). The SCAN + rVV10 functional was used, as it has been shown to have better performance for stacked two-dimensional (2D) materials [34] than other semiempirical methods for van der Waals correction, such as D3 or D3-BJ. Calculations using the vdW-opbB86b functional [35] were also performed for comparison. All periodic calculations were performed with the projected augmented wave pseudopotential [36, 37] for all atoms in restricted spin ISPIN = 1 (Zn(II) has zero spin). The plane-wave cut-off energy was set to 400 eV. The energy convergence criterion was set to 10^{-5} eV, with a maximum force per atom of 0.01 eV Å^{-1}. We used MOF unit cell parameters of 15 Å × 15 Å × 5.8 Å, as reported by Ahmad *et al* [23] for an idealized PDC SURMOF-2 with a tetragonal structure based on out-of-plane x-ray diffraction. MOF structure optimization was performed using 2 × 2 × 4 k-points with gamma points sampling for a fixed unit cell (all atoms were allowed to move) to retain the experimentally observed structural parameters.

Modeling of the Zn-PDC structures resulted in two most stable MOF structures, as shown in figures 2(a) and (b); these were validated by *ab initio* molecular dynamics simulations at 300 K for 2 ps. The SURMOF with tetrahedral Zn(II) node, **Zn-PDC-1** (figure 2(a)), was 0.83 eV more stable than the typical Zn-paddle-wheel-type node, **Zn-PDC-2** (figure 2(b)). The energetically unfavorable formation of **Zn-PDC-2** was connected to the twist of the COO$^-$ functional group [51] from the planarity of the perylene fragment of the PDC linker to form a Zn-paddle-wheel secondary building unit (SBU). In addition,
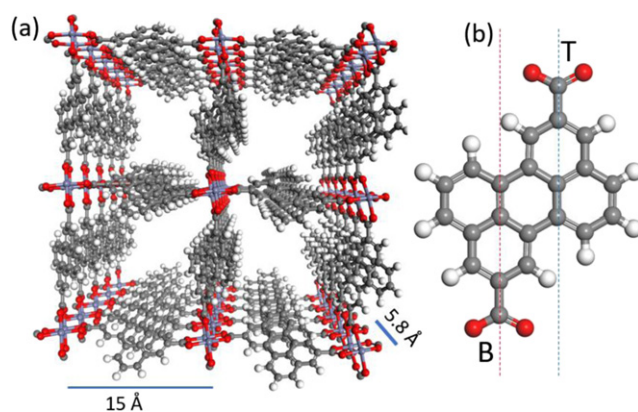
Figure 1. (a) Schematic representation of the Zn-PDC SURMOF-2 structure. (b) Optimized structure of the PDC linker with two axes (T, top, and B, bottom) for the coordination to the MOF metal node.

owing to the non-uni-axial axle of the linker to the SBU, COO$^-$ groups could not be connected by one axis to Zn(II) atoms and formed a tetrahedral instead of a square-planar coordination, as in the Zn-paddle-wheel SBU (figure S2). Both structures were characterized by the formation of perylene stacks with intermolecular distances of 3.38–3.42 Å. This enabled efficient structure stabilization via $\pi-\pi$ interactions (green areas in figure 2(c)), as calculated from the non-covalent interaction index [38] based on the electron density and reduced density gradient using NCIPLOT v.3.0 [39].

In-depth analysis of π-stacking patterns between neighboring perylene fragments in the optimized MOF structures revealed slight differences in the stacking of PDC. Stacking of linkers in the lowest minimum, **Zn-PDC-1** (figure 2(d), molecules in blue and green), consisted of aromatic ring stacking similar to the best $\pi-\pi$ interactions of a benzene dimer, i.e., parallel-displaced [52]. This resulted in the total interaction energy between two PDC linkers being 57.7 kJ mol^{-1} (table S1), as obtained by a supermolecular approach using B3LYP/def2-TZVP with DFT-D3 dispersion correction [40] and Becke–Johnson (BJ) damping [41]. Stacking in **Zn-PDC-2** was slightly different (molecules in red and green in figure 2(d)): the shift of the PDC planes by 0.6 Å resulted in sandwich-like stacking of edge-phenyl rings, with additional repulsion between quadrupole moments that lowered the interaction energy by 13.8 kJ mol^{-1}. Casanova [53] also observed such antibonding character and found that perfectly eclipsed perylene dimers had the least favorable binding energy. To investigate the impact of the stacking pattern of perylene chromophores on the electronic and optical properties of **Zn-PDC-1** and **Zn-PDC-2**, we extracted dimers of PDC linkers from periodically optimized structures and used them for further DFT calculations with the cluster approach. Only PDC fragments saturated by H atoms, without the Zn SBU, were considered.

All molecular calculations, including absorption and emission spectra, optimization of the lowest excited singlet state and vibrational analysis of PDC dimers, were performed using the hybrid B3LYP [42, 43] functional with the def2-TZVP [44, 45] basis set, and DFT-D3 dispersion correction [40]
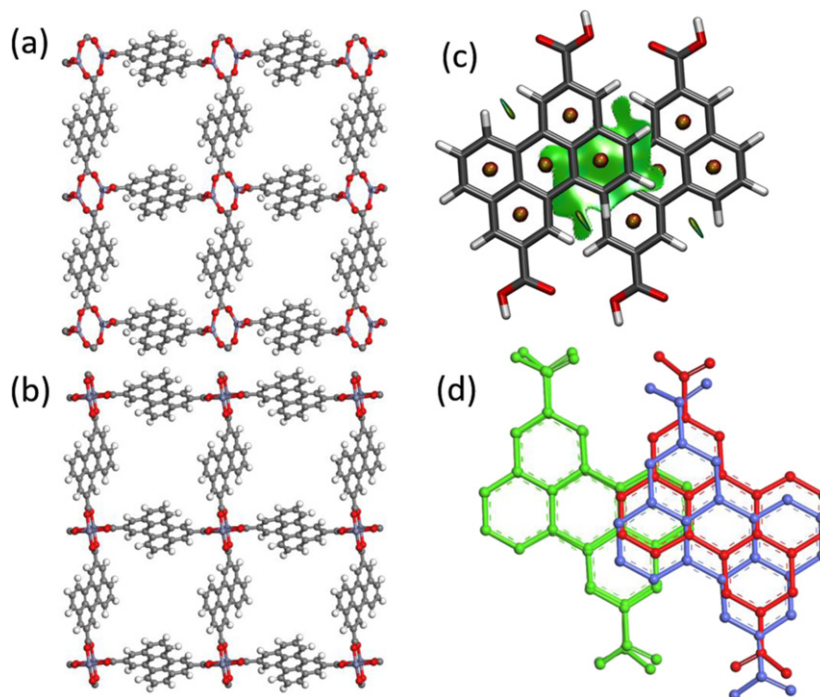
Figure 2. Optimized structures of Zn-PDC: (a) with Zn-carboxylate tetrahedral coordination, **Zn-PDC-1** (the global minimum); and (b) with tilted Zn-paddle-wheel, **Zn-PDC-2**. The relative energy difference between the structures is 0.83 eV. (c) $\pi-\pi$ interaction surface between the perylene molecules in a dimer (areas in green denote attractive $\pi-\pi$ interactions) obtained by NCIPLOT analysis [39]. Visualization was made with the isovalue of 0.3 a.u. (d) Out-of-plane view of the perylene stacking in **Zn-PDC-1** (perylene fragments in blue and green) and **Zn-PDC-2** (perylene fragments in red and green) in a dimer unit. The bottom molecules in green represent overlapping PDC molecules from both MOFs. Only the position of the top molecule changes and introduces effects discussed in the text.

with BJ damping [41], in TURBOMOLE v.7.4 [46]. Excited state properties were calculated using a time-dependent DFT (TD-DFT) approach. To retain the original connection of the PDC molecules in a dimer in the MOF scaffold, all calculations were performed with fixed O atoms. Exciton coupling was calculated using point dipole approximation with transition dipole moment (TDM) (see SI) for the singlet-singlet excitation of the corresponding PDC linker in **Zn-PDC-1** and **Zn-PDC-2**, and the orientation factor originated from the position of PDC in a dimer. To explicitly include the influence of the MOF polarization environment on the exciton coupling between linkers, we used our *ab initio* QuantumPatch [47–49] approach (B3LYP/def-SVP and B3LYP/def2-TZVP) with the SimStack workflow client. **Zn-PDC-1** and **Zn-PDC-2** MOFs consisting of 72 linker molecules (figure S7) were considered. Coupling of the central molecule (marked in red in figure S8) and PDC linkers in different orientations, accounting for partial charges within a radius of 25 Å, were calculated (table S3). The QuantumPatch approach was also used to calculate all microscopic parameters in the Marcus equation [50] (see SI) to estimate the electron and hole hopping transport in **Zn-PDC-1** and **Zn-PDC-2**. All possible PDC dimers within a radius of 25 Å were calculated, and parameters of the central PDC dimer (figures S6 and S7) were used for the prediction of charge carrier mobility.

Electronic properties of **Zn-PDC-1** and **Zn-PDC-2** arising from band-like transport were calculated with plane-wave DFT, using a k-points grid of $4 \times 4 \times 10$ for the Perdew–Burke–Ernzerhof (PBE) functional and $2 \times 2 \times 4$ for the

HSE06 functional with VASP 5.4.4. Explicit k-points for HSE band structures with a density of ten k-points per path (see SI) were implemented. Effective mass tensors were calculated by parabolic fitting at the minima of the valence and conduction bands.

3. Results and discussion

3.1. Photophysical properties of SURMOF

2D layers of a SURMOF-2-type structure, formed by linking a paddle-wheel-type node (SBU) and ditopic linker, were stacked in AA fashion along the [010] axis through van der Waals interactions, as illustrated in figure 1(a). The interlayer distance along the [010] axis was 0.58 nm, as revealed by the in-plane x-ray diffraction pattern [23]. Such closely spaced 2D-layers could potentially create ordered $\pi-\pi$ stacking along the [010] axis. In recent years, similar packing in various other chromophores has been realized, enabling efficient anisotropic energy transfer [11, 13], J-aggregated emission [12, 51], photon-upconversion [34], and indirect band-gap-like properties [34]. In the case of SURMOF-2, AA stacking and 3,9-substitution of perylene enforce a strong dipole–dipole interaction, as illustrated in figures 1(b) and S5, enabling exciton coupling between the neighboring molecules.

The ultraviolet–visible light (UV–vis) spectrum of the solvated PDC exhibited a maximum at 464 nm, with distinct vibronic character (figure 3(a)), whereas for SURMOF, a blueshifted maximum at 405 nm and a red-shifted broad shoulder
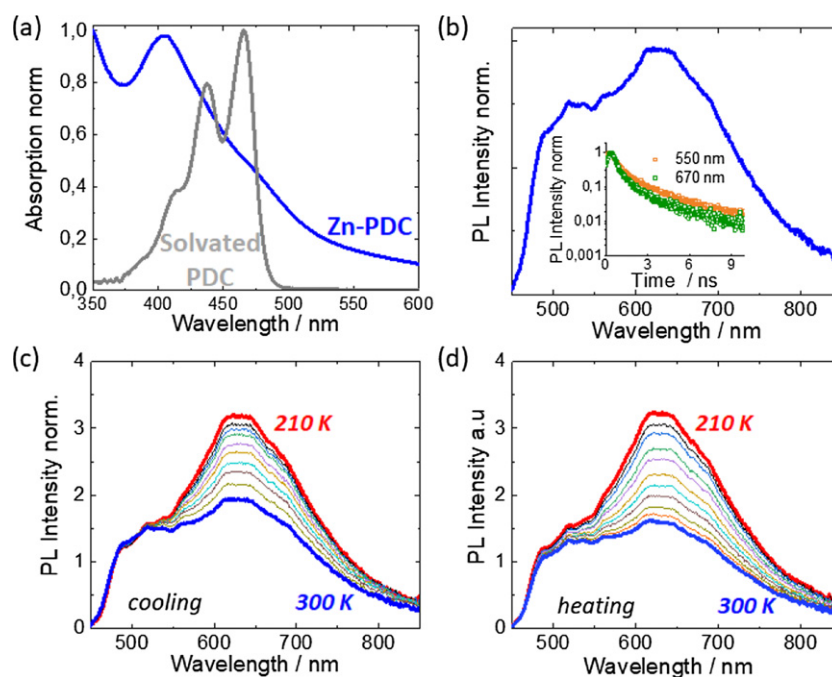
Figure 3. (a) Experimental UV−vis spectra of the solvated PDC linker (20 μM in ethanol) and SURMOF. The solvatochromic dependence of the spectra is depicted in figure S3; (b) emission spectrum and the fluorescence lifetime of SURMOF observed at 550 and 670 nm. Different PL decay confirms complex nature of the SURMOF emission; (c)−(d) temperature-dependent fluorescence spectra of the SURMOF-2 upon cooling and heating.

band at ∼460–510 nm were observed (figure 3(a)). As solvent polarity plays a major part in determining the ground state energy of perylene (figure S3), comparison of the absorption spectra of the solvated PDC (in ethanol, 20 μM) and SURMOF (dielectric constant ∼2–3) did not help us to understand the type of electronic coupling involved in SURMOF. The fluorescence spectrum recorded for SURMOF with excitation at 400 nm showed two distinct excited states: one at ∼520 nm with vibronic character; and another red-shifted at maximum ∼640 nm with broad character (figure 3(b)). Monitoring the fluorescence decay profiles at 550 and 670 nm indicated the long-lived nature of the broad red-shifted band, compared with the blue-shifted monomer-like emission at 520 nm (figure 3(b), inset). The broad featureless nature of the emission profile at 640 nm indicated excimer-like emission in SURMOF. The fact that these two excited states were very distinct in nature was evident from the temperature-dependent fluorescence data illustrated in figures 3(c) and (d). Whereas the blue-shifted monomer-like emission band remained nearly unaffected, the red-shifted emission exhibited pronounced change. These observations were surprising, considering that PDC is a structurally rigid molecule and the linker geometry in the SURMOF-2 structure was also severely constrained.

A previously studied anthracenedibenzoicacid (ADB)-linker-based [11] SURMOF-2 exhibited a similar dual excited state. However, the origin of its dynamic nature was attributed to the rotational flexibility present in the ADB linker. In the case of Zn-PDC, the rotation of the carboxyl groups coordinated to the metal node was non-uni-axial. Figure 1(b) shows two separate axes connecting linkers with an SBU, i.e., bottom (B) and top (T), marked with dashed red and blue lines,

which suppress twists of COO$^-$ groups during coordination to Zn-SBU. The energy barrier for such a non-uni-axial twist is predicted to be higher than those reported for typical MOF linkers, i.e. ∼0.5 eV [35, 36] (energy barrier for the COO$^-$ twist of the benzenedicarboxylate linker), resulting in different excited state dynamics of Zn-PDC compared with those reported for Zn-ADB.

In Zn-PDC, neighboring PDC molecules were localized at graphite-like intermolecular distances (3.38 Å; figures 1 and 4(c)), allowing strong π-stacking and van der Waals interactions between PDC linkers in the inter-sheet direction. These resulted in overlap and delocalization of the Frontier orbitals (figures 4(b) and S3) and, therefore, in a change in the spectral properties of Zn-PDC in comparison with the solvated molecule. Whereas the theoretically calculated (B3LYP/def2-TZVP) maximum peak of absorption of free PDC was at 437 nm (blue solid line in figure 4(a)), lying within the broad absorption peak obtained experimentally, absorption of PDC in a dimer unit of Zn-PDC was red-shifted by 76 meV and 26 meV (green solid line in figure 4(a)), with maxima at 449 nm and 441 nm, for **Zn-PDC-1** and **Zn-PDC-2**, respectively (figure S5). The observed red-shift can be attributed to the existence of PDC in the SURMOF in a J-aggregate form. In general, depending on the organizational pattern of perylene monomers—'face-to-face' (54.7° < θ < 90°), i.e., H-aggregate, or slipped, i.e., 'head-to-tail' (θ < 54.7°) J-aggregates—splitting of the singlet excited state into upper and lower transition states occurs. This shifts absorption bands to higher (hypsochromic shift) and lower (bathochromic shift)
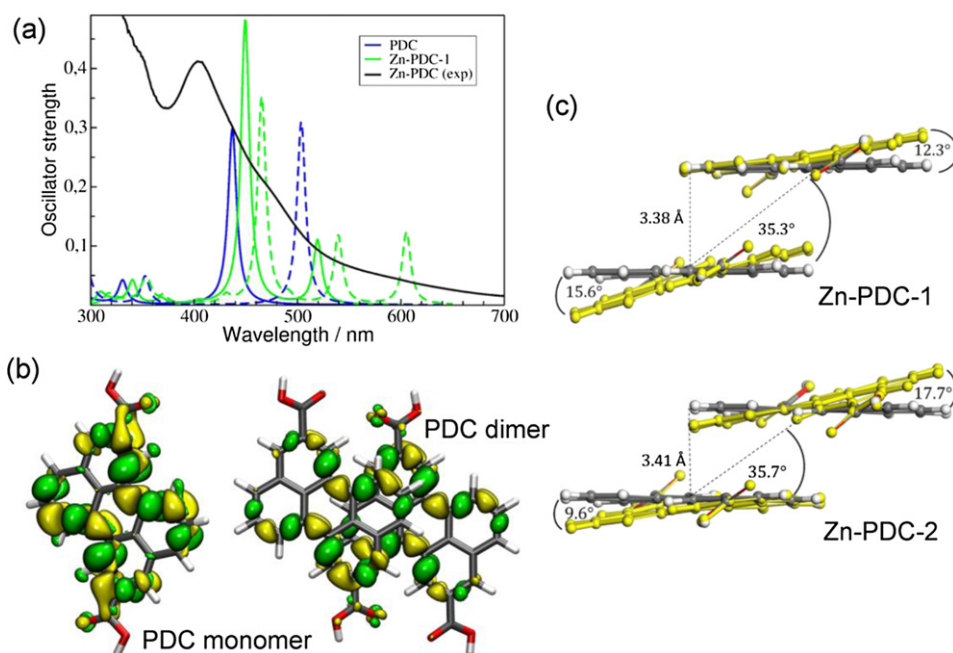
Figure 4. (a) Absorption (solid lines) and emission (dashed lines) spectra of the gas-phase PDC linker and the PDC dimer in **Zn-PDC-1** obtained with B3LYP/def2-TZVP. Experimentally measured UV–vis absorption spectrum of SURMOF (marked with the black solid line) is shown for comparison. (b) Electron density difference (isovalue of 0.0005 a.u.) upon singlet excitation of PDC monomer and dimer (electron accepting and donating areas are marked with yellow and green, respectively). (c) Ground-state PDC J-aggregates in MOF optimized using plane-wave DFT (gray) with superposed optimized first excited state geometries using TD-DFT (yellow), and angle between the lines connecting the geometrical centers of the PDCs in a dimer.

energy ranges [28, 52, 53] for the H- and J-aggregates, respectively. The calculated absorption spectra also showed low-energy bands at 519 nm (**Zn-PDC-1**) and 504 nm (**Zn-PDC-2**), typical of J-aggregates. These bands cannot be explicitly deduced from the experimental absorption spectrum owing to the broad absorption band as a result of closely spaced vibrational levels and molecular vibrations at room temperature [62, 63]. The bathochromic shift and J-band originated from strong coupling between the TDMs of the constituent molecules and, therefore, splitting of the singlet excited state and low-energy transition (figure S4). This process was enhanced by the relatively small angle of 35.3° between the TDM and the line connecting the geometrical centers of the perylene monomers in a dimer (figure 4(c)), leading to exciton coupling between stacking PDC molecules of -695 cm^{-1} and -416 cm^{-1} for **Zn-PDC-1** and **Zn-PDC-2**, respectively (table S3).

Interchromophoric interactions and strong J-type exciton coupling between perylene molecules in a dimer unit result in delocalization of the electronically excited state over many chromophores and, therefore, substantial changes in Zn-PDC emission properties. Whereas the highly ordered aggregation in SURMOF-2 and the close positions of the PDC chromophores trigger excimer states and dominant strong emission at 605 nm (green dashed line in figure 4(a)), typical of perylene excimers [22, 54, 55], the small emission peak at 539 nm may be attributed to J-aggregation or to the short-lived (within 150 ps [55]) fluorescent Y-state, reported in α-perylene crystals at ~530 nm [50]. The Y-state is a partially relaxed excited

molecular pair that activates the highly fluorescent excimer E-state with broad emission at lower energies [56, 57]; however, it has been shown to exist mostly at lower temperatures [58]. This fact, together with the temperature dependence of the ratio of the 0–0 and 0–1 emission bands [30, 59] (figures 3(c) and (d)), proves the J-type aggregation of PDC in a SURMOF.

The existence of a low-intensity, high-energy emission peak at $\lambda < 500$ nm can be attributed to monomer emission from molecules at the grain boundaries and in defects of the SURMOF. The insignificant contribution of monomeric states to the emission of SURMOF (figures 3(c) and (d)) suggests a highly ordered SURMOF structure with low defect concentration. This is supported by the similar temperature dependence of excimer emission on cooling and heating; an increase in emission upon temperature decrease, when molecular vibrations were slowed down enabling efficient exciton coupling, was observed. Similar temperature dependence has been reported for an α-perylene crystal structure [58] and investigated by Spano *et al* [30]. Notably, the observed differences in the stacking of **Zn-PDC-1** and **Zn-PDC-2** also induced differences in emission (figure S5): the excimer emission from the PDC dimer in **Zn-PDC-2** showed less red-shifted excimer emission (peak maximum at 591 nm) in comparison with the experimentally observed values (figures 3(c) and (d)). This suggests that the **Zn-PDC-1** structure better mimics PDC stacking in a SURMOF and is more probable to be found in the SURMOF structures formed in experiment. It also indicates that subtle modifications of the PDC linker, affecting the stacking pattern in a SURMOF, can dramatically change the photophysical
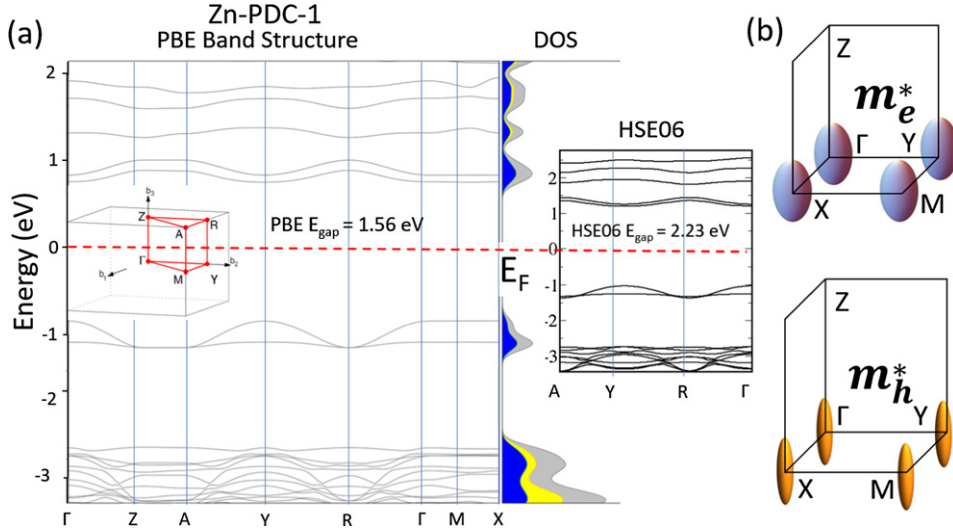
Figure 5. (a) Electronic band structure and density of states (DOS) of **Zn-PDC-1** using PBE and HSE06 functionals. Fermi energy is marked by the red dashed line. DOS in blue and yellow denote the contributions from s and p orbitals; the total DOS is shown in gray. (b) Visualization of the constant energy surface of the minima in the conduction band (top) and maxima in the valence band (bottom) for bare hole (1.89 m_o) and bare electron (6.9 m_o) effective mass. Extrema of the bands for the relevant effective mass calculations are at points Γ, Y, M, and X.

response of aggregates, enabling myriad further improvements in the design of new emissive devices [21, 51].

3.2. Semiconducting properties of Zn-PDC

The highly ordered and defect-free structure of SURMOF is especially relevant to charge carrier transport. To demonstrate the semiconducting nature of Zn-PDC and predict charge carrier mobility, a systematic analysis of the electronic structure of the Zn-PDC SURMOF was performed. The band structures of **Zn-PDC-1** and **Zn-PDC-2** are shown in figures 5 and S8. Both the PBE functional and the more accurate hybrid HSE06 functional were used to calculate the electronic band structures. The band dispersion was the same within the two functionals; only the band gaps were different. GGA functionals underestimate band gap, consistent with previous investigations [60, 61]. The direct band gap values for **Zn-PDC-1** were 1.56 eV (PBE) and 2.23 eV (HSE06). The latter agrees with the band gap obtained experimentally (figure S10). This enables SURMOF to be applied in visible light-activated charge transport.

The band structure diagram showed strong dispersion when the lattice momentum of electrons in the z direction (Δk_z) changed (paths Γ–Z and A–Y–R–Γ), relative to the normal vector of the inter-sheet stacking in Zn-PDC SURMOF-2. The lowest effective mass tensor components m^*_{zz} (see SI), calculated from the extrema of the valence and conduction bands (Γ, Y, M, X), for bare holes and bare electrons were 1.89 m_o and 6.9 m_o, respectively (where m_o is the electron mass). The **Zn-PDC-2** structure had indirect band gap (figure S9) values of 1.78 eV (PBE) and 2.31 eV (HSE06). Here, the effective mass of electrons (2.93 m_o) was smaller than that of holes (26.3 m_o). This suggests that **Zn-PDC-1** is a p-type semiconductor, whereas **Zn-PDC-2** is n-type. The finite effective mass in the k_z direction translates to the possible conductivity

through delocalized π–π orbitals perpendicular to the perylene plane, i.e., charge carrier conductivity between stacked perylene linkers. This observation was directly influenced by the close positioning of linkers (3.38 Å) and strong stacking interactions (figure 2(c)). The dispersion of the valence and conduction bands when k_z was constant was flat (Z–A and Γ–M–X). This is related to the high effective mass of the charge carriers in the k_x and k_y directions (figures 5(b) and S9(b)), resulting in confinement of charge carriers upon movement on the PDC plane. Therefore, the conduction behavior of **Zn-PDC-1** and **Zn-PDC-2** had a pronounced anisotropic nature. Indeed, owing to the highly anisotropic effective mass tensor (small m^*_{zz}, large $m^*_{xx}, m^*_{yy}, m^*_{xy}$), conduction might have been limited by percolation through crystal grains in the k_z direction [62], hindering conventional band-like transport properties. The latter, together with the large distances between linkers in other than in the stacking direction in the Zn-PDC, resulted in higher electron/hole localization. Therefore, charge hopping transport is more probable than band-like transport.

The charge hopping rates for both Zn-PDC (table S4), calculated using the Marcus theory of electron transport with the QuantumPatch approach (section 2.2 and figures S7 and S8), also suggest different conduction mechanisms in **Zn-PDC-1** and **Zn-PDC-2** as a function of π–π interactions between perylene molecules in a dimer unit. Whereas **Zn-PDC-1** had relatively good p-type charge carrier mobilities, μ, with more than six times higher hole ($\mu = 7.34$ cm^2 Vs^{-1}) than electron ($\mu = 1.16$ cm^2 Vs^{-1}) transport, **Zn-PDC-2** was an n-type material with predicted hole mobility of $\mu = 6.00 \times 10^{-4}$ cm^2 Vs^{-1}, three orders of magnitude lower than that of electrons ($\mu = 6.80 \times 10^{-1}$ cm^2 Vs^{-1}). Differences in the transport mechanisms of SURMOFs with the same chemical composition but slightly different SBU geometries are mainly due to the different electron coupling matrix

elements between perylene linkers as a function of their interchromophoric π-orbital overlap. With different transport mechanisms, band-like and hopping, Zn-PDC showed similar semiconducting properties; however, owing to its anisotropic 1D-delocalized nature, the charge carrier mobility was one order of magnitude lower than that of α-perylene crystal [63]. However, the modulation of semiconducting properties of Zn-PDC using the SURMOF-2 strategy is straightforward, and further improvements will be reported.

4. Conclusions

We have demonstrated the excited state properties of crystalline PDC chromophores assembly in a SURMOF-2, Zn-PDC. Owing to the long-range order and controllable inter-sheet stacking between the perylene linkers in the MOF, we observed two different excited states. Structure prediction of Zn-PDC by periodic DFT and in-depth analyses of its spectroscopic properties using TD-DFT revealed the existence of a J-aggregate type assembly of perylene. This enabled strong exciton coupling, leading to delocalization of the electronically excited state over many chromophores and, therefore, intense excimer emission with an extrinsic monomer contribution.

We have used rigorous electronic structure analyses to investigate the sensitivity of MOF photophysics as a function of linker orientation and $\pi-\pi$ interactions. MOFs with the same chemical composition but slight structural deviations in SBUs showed differences in spectroscopic and semiconducting properties of Zn-PDC. The perylene-based MOF with tetrahedral Zn coordination better mimicked the emission and band gap characteristics of the film obtained experimentally, having good p-type conduction with mobility of 7.34 cm^2 Vs^{-1}. Owing to higher repulsion interactions between perylene linkers in the conventional Zn-paddle-wheel MOF, it showed less red-shifted emission and was characterized by n-type conduction with electron effective mass of 2.93 m_o, as calculated from the electronic band structure, and electron mobility of 0.68 cm^2 Vs^{-1}, obtained using Marcus hopping transport.

Our investigations illustrate the impact of linker orientation on interchromophore interactions, where a subtle interplay of electronic coupling results in diverse functions of the MOF thin film. The use of MOFs as highly tunable molecular architectures enables virtual molecular engineering with *ab initio* quantum mechanical calculations towards tailoring MOFs for the desired functionality. This constitutes a key milestone in the establishment of design rules and patterns for functionalization to improve optoelectronic device efficiency.

ORCID iDs

Mariana Kozlowska https://orcid.org/0000-0001-8471-8914
Yohanes Pramudya https://orcid.org/0000-0002-0950-7655
Shahriar Heidrich https://orcid.org/0000-0002-9691-4012
Bryce S Richards https://orcid.org/0000-0001-5469-048X
Christof Wöll https://orcid.org/0000-0003-1078-3304
Ritesh Haldar https://orcid.org/0000-0001-9697-9169

References

[1] Zhu L, Al-Kaysi R O, Dillon R J, Tham F S and Bardeen C J 2011 *Cryst. Growth Des.* **11** 4975–83
[2] Hu Z, Willard A P, Ono R J, Bielawski C W, Rossky P J and Vanden Bout D A 2015 *Nat. Commun.* **6** 8246
[3] Haldar R, Heinke L and Wöll C 2020 *Adv. Mater.* **32** 1905227
[4] Furukawa H, Cordova K E, O'Keeffe M and Yaghi O M 2013 *Science* **341** 1230444
[5] Kitagawa S, Kitaura R and Noro S-I 2004 *Angew. Chem., Int. Ed.* **43** 2334–75
[6] Pramudya Y and Mendoza-Cortes J L 2016 *J. Am. Chem. Soc.* **138** 15204–13
[7] Li H, Wang K, Sun Y, Lollar C T, Li J and Zhou H-C 2018 *Mater. Today* **21** 108–21
[8] Sumida K, Rogow D L, Mason J A, McDonald T M, Bloch E D, Herm Z R, Bae T-H and Long J R 2012 *Chem. Rev.* **112** 724–81
[9] Kapelewski M T *et al* 2018 *Chem. Mater.* **30** 8179–89
[10] Li J-R, Sculley J and Zhou H-C 2012 *Chem. Rev.* **112** 869–932
[11] Zhu L, Liu X-Q, Jiang H-L and Sun L-B 2017 *Chem. Rev.* **117** 8129–76
[12] Yang D and Gates B C 2019 *ACS Catal.* **9** 1779–98
[13] (a)Kreno L E, Leong K, Farha O K, Allendorf M, Van Duyne R P and Hupp J T 2012 *Chem. Rev.* **112** 1105–25
(b)Jiang W, Liu Z, Mei J-W, Cui B and Liu F 2019 *Nanoscale* **11** 955–61
[14] Stavila V, Talin A A and Allendorf M D 2014 *Chem. Soc. Rev.* **43** 5994–6010
[15] Liu X *et al* 2019 *Angew. Chem., Int. Ed.* **58** 9590–5
[16] Haldar R *et al* 2019 *Nat. Commun.* **10** 1–7
[17] Adams M *et al* 2019 *ACS Appl. Mater. Interfaces* **11** 15688–97
[18] (a)Virmani E, Rotter J M, Mähringer A, von Zons T, Godt A, Bein T, Wuttke S and Medina D D 2018 *J. Am. Chem. Soc.* **140** 4812–9
(b)Falcaro P *et al* 2017 *Nat. Mater.* **16** 342–8
(c)Stassen I *et al* 2016 *Nat. Mater.* **15** 304–10
(d)Liu J and Wöll C 2017 *Chem. Soc. Rev.* **46** 5730–70
[19] Heinke L and Wöll C 2019 *Adv. Mater.* **31** 1806324
[20] Li J *et al* 2020 *ACS Appl. Mater. Interfaces* **12** 26727–32
[21] Seco J M *et al* 2018 *Sci. Rep.* **8** 14414

[22] Sikdar N, Dutta D, Haldar R, Ray T, Hazra A, Bhattacharyya A J and Maji T K 2016 *J. Phys. Chem.* C **120** 13622–9

[23] Ahmad S, Liu J, Gong C, Zhao J and Sun L 2018 *ACS Appl. Energy Mater.* **1** 249–53

[24] Quah H S, Chen W, Schreyer M K, Yang H, Wong M W, Ji W and Vittal J J 2015 *Nat. Commun.* **6** 7954

[25] Liu J *et al* 2012 *Sci. Rep.* **2** 921

[26] Haldar R *et al* 2017 *Chem. Eur. J.* **23** 14316–22

[27] Haldar R *et al* 2018 *Nat. Commun.* **9** 4332

[28] Hestand N J and Spano F C 2017 *Acc. Chem. Res.* **50** 341–50

[29] Oleson A *et al* 2019 *J. Phys. Chem.* C **123** 20567–78

[30] Kistler K A, Pochas C M, Yamagata H, Matsika S and Spano F C 2012 *J. Phys. Chem.* B **116** 77–86

[31] Sun J, Ruzsinszky A and Perdew J P 2015 *Phys. Rev. Lett.* **115** 036402

[32] Sun J *et al* 2016 *Nat. Chem.* **8** 831–6

[33] Kresse G and Hafner J 1993 *Phys. Rev.* B **47** 558–61

[34] Peng H, Yang Z-H, Perdew J P and Sun J 2016 *Phys. Rev.* X **6** 041005

[35] Klimeš J, Bowler D R and Michaelides A 2011 *Phys. Rev.* B **83** 195131

[36] cms.mpi.univie.ac.at/vasp/vasp/Recommended_PAW_potentials_DFT_calculations_using_vasp_5_2.html

[37] Kresse G and Joubert D 1999 *Phys. Rev.* B **59** 1758–75

[38] Johnson E R, Keinan S, Mori-Sánchez P, Contreras-García J, Cohen A J and Yang W 2010 *J. Am. Chem. Soc.* **132** 6498–506

[39] Contreras-García J, Johnson E R, Keinan S, Chaudret R, Piquemal J-P, Beratan D N and Yang W 2011 *J. Chem. Theory Comput.* **7** 625–32

[40] Grimme S, Antony J, Ehrlich S and Krieg H 2010 *J. Chem. Phys.* **132** 154104

[41] Grimme S, Ehrlich S and Goerigk L 2011 *J. Comput. Chem.* **32** 1456–65

[42] Becke A D 1993 *J. Chem. Phys.* **98** 5648–52

[43] Lee C, Yang W and Parr R G 1988 *Phys. Rev.* B **37** 785–9

[44] Schäfer A, Horn H and Ahlrichs R 1992 *J. Chem. Phys.* **97** 2571–7

[45] Weigend F and Ahlrichs R 2005 *Phys. Chem. Chem. Phys.* **7** 3297

[46] Balasubramani S G *et al* 2020 *J. Chem. Phys.* **152** 184107

[47] Friederich P, Meded V, Symalla F, Elstner M and Wenzel W 2015 *J. Chem. Theory Comput.* **11** 560–7

[48] Friederich P, Symalla F, Meded V, Neumann T and Wenzel W 2014 *J. Chem. Theory Comput.* **10** 3720–5

[49] Friederich P, Coehoorn R and Wenzel W 2017 *Chem. Mater.* **29** 9528–35

[50] Marcus R A 1993 *Rev. Mod. Phys.* **65** 599

[51] Haldar R, Fu Z, Joseph R, Herrero D, Martín-Gomis L, Richards B S, Howard I A, Sastre-Santos A and Wöll C 2020 *Chem. Sci.* **11** 8626

[52] Herbst S, Soberats B, Leowanawat P, Stolte M, Lehmann M and Würthner F 2018 *Nat. Commun.* **9** 2646

[53] Lim J M, Kim P, Yoon M-C, Sung J, Dehm V, Chen Z, Würthner F and Kim D 2013 *Chem. Sci.* **4** 388–97

[54] Bairi P, Roy B and Nandi A K 2011 *RSC Adv.* **2** 264–72

[55] Seko T, Ogura K, Kawakami Y, Sugino H, Toyotama H and Tanaka J 1998 *Chem. Phys. Lett.* **291** 438–44

[56] Martyński T, Hertmanowski R, Stolarski R and Bauman D 2008 *Thin Solid Films* **516** 8834–8

[57] Nakagawa K, Numata Y, Ishino H, Tanaka D, Kobayashi T and Tokunaga E 2013 *J. Phys. Chem.* A **117** 11449–55

[58] Walker B, Port H and Wolf H C 1985 *Chem. Phys.* **92** 177–85

[59] Lefler K M, Brown K E, Salamant W A, Dyar S M, Knowles K E and Wasielewski M R 2013 *J. Phys. Chem.* A **117** 10333–45

[60] Endres R G, Fong C Y, Yang L H, Witte G and Wöll C 2004 *Comput. Mater. Sci.* **29** 362–70

[61] Sharifzadeh S, Biller A, Kronik L and Neaton J B 2012 *Phys. Rev.* B **85** 125307

[62] Devdariani A Z, Demidov V I, Kolokolov N B and Rubtsov V I 1983 *Sov. Phys. - JETP* **57** 960–4

[63] Datta A, Mohakud S and Pati S K 2007 *J. Mater. Chem.* **17** 1933–8